Coherent response to optical excitation in a strongly absorbing rare-earth ion-doped crystal

J. Ruggiero, T. Chanelière, and J.-L. Le Gouët*

Laboratoire Aimé Cotton, Bâtiment 505, Campus Universitaire, 91405 Orsay Cedex, France
**Corresponding author: jean-louis.legouet@lac.u-psud.fr*

Received September 14, 2009; accepted October 27, 2009;
posted October 29, 2009 (Doc. ID 117087); published December 11, 2009

We investigate coherent propagation through a large optical density Tm^{3+}:YAG crystal. Using an ultrastable laser, fiber filtering, and site selection, we investigate the transmitted pulse temporal profile. The plane-wave condition is satisfied by selection of the illuminated-spot central area. We pay special attention to π pulse transmission in the prospect of implementing optical quantum storage protocols. © 2009 Optical Society of America

OCIS codes: 020.1670, 160.5690, 190.5530, 270.6630.

1. INTRODUCTION

The coherent response to optical excitation has been investigated for a long time. Actually, mere linear absorption of an optical beam through a material slab represents the most elementary manifestation of this feature. Indeed, the transmitted beam results from a coherent combination of the incident field and the instantaneous material response. It has also been realized early that a coherent optical response is related to the collective quantum excitation of an atomic ensemble. As pointed out by R. Dicke [1], *all the molecules are interacting with a common radiation field and hence cannot be treated as independent*. However, a semiclassical treatment is generally adequate to describe the coherent response [1], especially if the number of atoms per λ cube is small enough so that superfluorescence cannot start up on the experiment time scale [2]. In the framework of the semiclassical description, McCall and Hahn were able to derive an area theorem that accounts for the propagation of an arbitrary intensity pulse through an arbitrary optical density slab [3], giving rise to the notion of self-induced transparency (SIT). To be coherent, the process must take place on a time scale much shorter than the atomic superposition state lifetime. Experimental demonstration in the nanosecond range was performed at once in both solids and atomic vapors at room temperature [3–5]. The McCall and Hahn theorem only predicts the pulse area behavior. For a more detailed description, especially to investigate the pulse deformation, one has to solve the Maxwell–Bloch (MB) equation numerically.

The connection with solitons has stimulated interest in SIT. It was shown [6] that a 2 π area pulse with a hyperbolic secant temporal profile can propagate without alteration through an absorbing medium. The breakdown of large area pulses into 2 π area components was also predicted [6] and observed [4,5]. A couple of decades later, the discovery of electromagnetically induced transparency (EIT) in ensembles of three-level atoms [7] renewed interest in the coherent response of optically thick media. Actually, a variety of induced transparency processes have been investigated in three-level systems [8,9]. The interplay of EIT with SIT was also considered [10,11]. In recent years, effort has been directed to the ultrashort pulse regime, where the usual assumptions, such as the rotating wave and slowly varying envelope approximations, may not be valid [12].

Rare-earth ion-doped crystals (REIC) represent an excellent test bed for coherent optical response investigation. Most of the limitations pointed out by Slusher in his review paper on SIT [13] are relaxed in these materials. The superposition state lifetime may reach hundreds of microseconds and is not limited by a transit time across the light beams. No diffusive motion can affect the spatial phase of the atomic states. The inhomogeneous broadening can be considered as infinite. Generally, the level degeneracy is completely lifted by the crystal field so that the ions behave as true two-level atoms on the propagation time scale. Other features depend on the specific host matrix. In yttrium aluminium garnet (YAG, $Y_3Al_5O_{12}$) for instance, the D_2 symmetry of substitution sites forbids the existence of permanent dipole moments. As a consequence, relaxation processes such as optical excitation-induced instantaneous spectral diffusion (ISD) are strongly reduced. In this matrix, appropriate crystal cutting and adequate polarization orientation make ions in different sites interact with the same dipole moment projection on the incoming field [14].

Coherent interactions in strongly absorbing REIC currently receive considerable attention due to prospects of these materials as a base for quantum memories. However, very few SIT coherent propagation data have been collected in REIC [15,16]. Reference [16] reports on experimental work in Tm^{3+}:YAG. However, inserting the sample in a cavity makes the quantitative analysis more difficult. In addition, coherent excitation conditions are not clearly satisfied since the laser is not stabilized. The same flaw affects the results in [11], where the interplay of EIT and SIT is evoked in the context of quantum stor-

age of light. In [15], propagation is investigated in Pr^{3+}:YSO. The laser is properly stabilized, but an unexpected low-transmission factor is observed.

In the present paper our aim is twofold. First, we reexamine the MB equation and propose a solution that analytically accounts for the instantaneous part of the atomic response. This fast component spreads over a broad spectral interval and complicates the numerical solution when the absorption line is strongly inhomogeneously broadened. Second, we present a detailed experimental investigation of coherent pulse propagation in a large optical density Tm^{3+}:YAG crystal at liquid helium temperature.

The paper is organized as follows. In Section 2 we present the original aspects of our MB equation solution. In Section 3 we review the main features of pulse propagation through a strongly absorbing medium as predicted by the MB equation. The experimental setup is described in Section 4. We present and discuss the experimental data in Section 5.

2. THE INSTANTANEOUS RESPONSE

The MB equation has been the object of intense theoretical and numerical investigation for many decades by both physicists and mathematicians. We do not intend to bring any new result in this extremely well-documented field. Instead, we rely on physical arguments in order to simplify the computation procedure. Specifically, we show that one can simply account for the contribution from atoms far from resonance. This way, the sum over the inhomogeneous width can be limited to a narrower spectral interval. To the best of our knowledge, this approach was not adopted before.

Let us consider a spatially and spectrally uniform distribution of two-level atoms. Spectral uniformity means that the inhomogeneous width of the optical transition is infinite. Let a monochromatic plane wave be directed to the sample. At the input side $z=0$, the electric field E(z, t) reads as

$$\mathrm{E}(0,t) = \mathrm{A}(0,t)\cos(\omega_L t + \varphi), \tag{1}$$

where φ is time independent. Within the frame of the slowly varying amplitude (SVA) and rotating wave (RWA) approximations, the MB equations read as follows:

$$\begin{aligned}
\partial_z \Omega(z,t) &= -\frac{\alpha}{2\pi}\int \mathrm{d}\omega_{ab}\,\mathrm{v}(\omega_{ab};z,t),\\
\partial_t \mathrm{u}(\omega_{ab};z,t) &= -\Delta \mathrm{v}(\omega_{ab};z,t),\\
\partial_t \mathrm{v}(\omega_{ab};z,t) &= -\Omega(z,t)\mathrm{w}(\omega_{ab};z,t) + \Delta \mathrm{u}(\omega_{ab};z,t),\\
\partial_t \mathrm{w}(\omega_{ab};z,t) &= \Omega(z,t)\mathrm{v}(\omega_{ab};z,t),
\end{aligned} \tag{2}$$

where $\Delta=\omega_{ab}-\omega_L$, and where $\Omega(z,t)$, $\mathrm{u}(\omega_{ab};z,t)$, $\mathrm{v}(\omega_{ab};z,t)$, and $\mathrm{w}(\omega_{ab};z,t)$represent the Rabi frequency and the components of the Bloch vector $\mathrm{B}(\omega_{ab};z,t)$, respectively. Let L represent the sample thickness. To further simplify the problem, we assume that the incoming pulse evolution characteristic time, i.e., the inverse spectral width $1/\Delta_p$, is much longer than L/c. Therefore we can neglect the time derivative $\partial_t\Omega(z,t)/\mathrm{c}$ in the wave equation.

To solve the equations numerically, one would like to get the spatial distribution $\Omega(z,t)$ at time t in terms of $\Omega(0,t)$, the boundary value at the sample input and of $\mathrm{B}(\omega_{ab};z,t-\tau)$, where $\tau\Delta_p \ll 1$. Then one would solve the Bloch equation at time t, starting with $\mathrm{B}(\omega_{ab};z,t-\tau)$ and $\Omega(z,t-\tau)$. It should be stressed that the material response at time t cannot be simply expressed in terms of the Bloch vector at $t-\tau$. Indeed, due to the infinite inhomogeneous bandwidth, the material gives rise to an instantaneous response. Let us formally solve the Bloch equation in the following way:

$$\begin{aligned}
\mathrm{v}(\omega_{ab};z,t) = \mathrm{v}(\omega_{ab};z,t-\tau)\cos(\Delta\tau) + \mathrm{u}(\omega_{ab};z,t-\tau)\sin(\Delta\tau)\\
-\int_0^\tau \Omega(z,t-\tau')\mathrm{w}(\omega_{ab};z,t-\tau')\cos(\Delta\tau')\mathrm{d}\tau'.
\end{aligned} \tag{3}$$

The first two terms on the right-hand side correspond to the free precession of the Bloch vector from $t-\tau$ to t. The last term reflects the coupling to the field during this time interval. Initially $\mathrm{w}(\omega_{ab};z,t_0)=-1$, since all the atoms sit in the ground state. As the pulse propagates through the sample, $\mathrm{w}(\omega_{ab};z,t)+1$ departs from 0 over a spectral interval given by the pulse width Δ_p. However, according to Eq. (3), the driving field uniformly excites the atoms all over the inhomogeneous width, since the weight factor $\mathrm{w}(\omega_{ab};z,t_0)$ is initially close to -1 everywhere. Summing over an infinite inhomogeneous width clearly raises a numerical computation issue. An infinite width contribution also reflects an instantaneous response feature that we intend to express analytically, thus relaxing the computation problem. Substituting $\mathrm{v}(\omega_{ab};z,t)$ into the wave equation one obtains

$$\begin{aligned}
\partial_z\Omega(z,t) = &-\frac{\alpha}{2\pi}\int \mathrm{d}\omega_{ab}\int_0^\tau \Omega(z,t-\tau')\cos(\Delta\tau')\mathrm{d}\tau'\\
&+\frac{\alpha}{2\pi}\int \mathrm{d}\omega_{ab}\int_0^\tau \Omega(z,t-\tau')[\mathrm{w}(\omega_{ab};z,t)\\
&+1]\cos(\Delta\tau')\mathrm{d}\tau' - \frac{\alpha}{2\pi}\int \mathrm{d}\omega_{ab}\mathrm{v}_{free}(\omega_{ab};z,t-\tau,t),
\end{aligned} \tag{4}$$

where:

$$\begin{aligned}
\mathrm{v}_{\mathrm{free}}(\omega_{ab};z,t-\tau,t) = \mathrm{v}(\omega_{ab};z,t-\tau)\cos(\Delta\tau)\\
+\mathrm{u}(\omega_{ab};z,t-\tau)\sin(\Delta\tau).
\end{aligned} \tag{5}$$

The instantaneous response contribution has been isolated in the first term on the right-hand side. This easily reduces to $-(\alpha/2)\Omega(z,t)$. The second term, of order $-(\alpha/2)\Delta_p\tau\Omega(z,t)$, can be neglected since $\Delta_p\tau \ll 1$. Finally the wave equation solution reads as

$$\Omega(z,t) = \Omega(0,t)e^{-\alpha z/2} - \frac{\alpha}{2\pi}\int_0^z dz' e^{-\alpha(z-z')/2}\int d\omega_{ab} v_{free}(\omega_{ab};z',t-\tau,t). \quad (6)$$

In the small area limit, the second term on the right-hand side can be neglected. The equation then reduces to the Bouguer law of absorption [17]. As a starting point for numerical computation, the equation conveniently expresses $\Omega(z,t)$ in terms of $\Omega(0,t)$ and of $B(\omega_{ab};z,t-\tau)$. In order to get $B(\omega_{ab};z,t)$ in terms of $B(\omega_{ab};z,t-\tau)$ and $\Omega(z,t-\tau)$, one complements Eq. (3) with the integral solutions for $u(\omega_{ab};z,t)$ and $w(\omega_{ab};z,t)$:

$$u(\omega_{ab};z,t) = u_{free}(\omega_{ab};z,t-\tau,t) + \int_0^\tau \Omega(z,t-\tau')w(\omega_{ab};z,t-\tau')\sin(\Delta\tau')d\tau',$$

$$w(\omega_{ab};z,t) = w(\omega_{ab};z,t-\tau) + \int_0^\tau \Omega(z,t-\tau')v(\omega_{ab};z,t-\tau')d\tau', \quad (7)$$

where

$$u_{free}(\omega_{ab};z,t-\tau,t) = u(\omega_{ab};z,t-\tau)\cos(\Delta\tau) - v(\omega_{ab};z,t-\tau)\sin(\Delta\tau). \quad (8)$$

According to Eq. (7), the second term on the right-hand side of Eq. (6) still apparently contains far-from-resonance contributions. Indeed, $u(\omega_{ab};z,t)$ and $v(\omega_{ab};z,t)$ are built from $v(\omega_{ab};z,t)$ all over the infinite inhomogeneous width. To show the instantaneous response is actually contained in the first term, let us define the new variables:

$$U(\omega_{ab};z,t) = u(\omega_{ab};z,t) + \int_0^\infty \Omega(z,t-\tau')\sin(\Delta\tau')d\tau',$$

$$V(\omega_{ab};z,t) = v(\omega_{ab};z,t) - \int_0^\infty \Omega(z,t-\tau')\cos(\Delta\tau')d\tau'. \quad (9)$$

Those new variables vanish far from resonance with the driving field. Then one easily verifies that Eq. (6) is left unchanged if $u(\omega_{ab};z,t-\tau)$ and $v(\omega_{ab};z,t-\tau)$ are respectively replaced by $U(\omega_{ab};z,t-\tau)$ and $V(\omega_{ab};z,t-\tau)$.

3. PULSE DISTORSION AND AREA THEOREM

According to the McCall and Hahn theorem [3], the transmitted pulse area, A_{out}, can be expressed in terms of the incoming pulse, A_{in}, as

$$\tan(A_{out}/2) = e^{-\alpha L/2}\tan(A_{in}/2), \quad (10)$$

where the pulse area is defined as $A = \int \Omega(t)dt$. The corresponding variation of the transmission factor A_{out}/A_{in} as a function of A_{in} is displayed in Fig. 1.

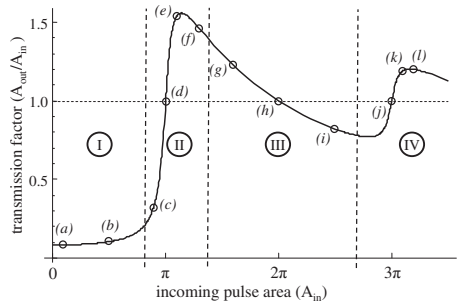

Fig. 1. Area theorem: pulse area transmission factor A_{out}/A_{in} as a function of the incoming pulse area A_{in}. Labels (a) to (l) refer to the different input-area conditions considered in Fig. 2.

To explore the shape distortion of an incoming rectangular pulse, we numerically solve the MB equations along the lines exposed in Section 2. The results of this computation are presented in Fig. 2 for different pulse area values. The box labels help to locate the propagation regime in Fig. 1. The distortion can be understood in light of the area theorem and of energy conservation. Four different regions can be identified in Fig. 1. In region (I) nearly no light is emitted after the incoming pulse extinction. The pulse simply obeys the Bouguer law and is hardly distorted. In region (II), located around π area, the pulse stretches in order to comply with two contradictory prescriptions. On the one hand the energy absorption increases, since all the resonantly excited atoms are promoted to the upper level, at any depth within the sample. On the other hand the area transmission factor grows larger that unity. Region (III) is centered on the 2 π area. The transmission factor is still close to unity, but less energy is absorbed since the resonantly excited atoms are returned to their ground state. In this region the outgoing pulse duration decreases, getting closer to that of the incoming pulse. In this region the pulse tends to the ex-

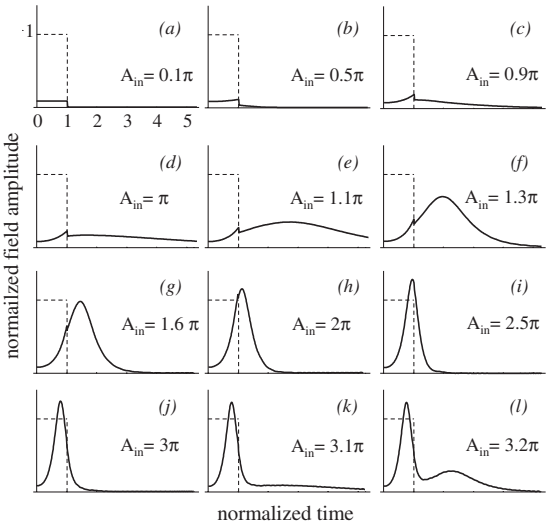

Fig. 2. Numerical solution of the MB equation. The incoming rectangular pulse (dotted line) propagates through an $\alpha L = 5$ sample. The temporal profile of the pulse at the output (solid line) is displayed for different values of the input area. Time and outgoing pulse amplitude are normalized to the duration and the amplitude of the incoming pulse, respectively. The box labels refer to the corresponding area values, as predicted by the McCall and Hahn theory in Fig. 1.

pected soliton hyperbolic secant shape. Finally the pulse area undergoes another increase in region (IV), around the 3 π area. As in region (II), this area increase conflicts with the energy depletion by the resonantly excited atoms that are left in the upper level. This apparent contradiction is solved by the emergence of a stretched secondary component in the tail of the main pulse. However, the 3 π pulse is less distorted than the π pulse by the increase of energy transfer to the atoms. Indeed, to excite the same number of atoms, a 3 π pulse consumes a 9 times smaller fraction of the available energy than a π pulse.

The rapid growing of the long tails, in both the π and 3 π regions, provides us with key features for experimental data analysis.

4. EXPERIMENTAL SETUP

The 0.5% at. Tm^{3+}:YAG crystal is cooled down to $\cong$2.2 K in a helium bath cryostat. The experiment is performed on the $^3H_4-^3H_6$ transition at 793 nm. The sample length is $L=5$ mm. At the operating temperature the opacity is measured to be $\alpha L \cong 5$. The crystal sides are cut perpendicular to direction [1, −1, 0], and the light beam is polarized along direction [1, 1, 1]. This way, three sites out of six interact with the driving field, and they do so with the same Rabi frequency.

The sample is excited by a monochromatic semiconductor laser (Fig. 3). We carefully control the spectro-temporal and spatial properties of the source. The laser linewidth is first reduced to less than 1 kHz by Pound–Drever–Hall locking to a high-finesse Fabry–Perot cavity. After a boost up through a tapered semiconductor amplifier, the laser beam is precisely temporally shaped by an acousto-optic modulator (AOM). The AOM is directly driven by a high-frequency arbitrary waveform generator (Tektronix AWG520) operating at 1 Gs/s, which guarantees precise amplitude and phase control. The beam is then spatially filtered by a 2 m long single-mode optical fiber.

The experimental conditions must be consistent with the plane-wave assumption of the theory. First we make the laser beam depth of field (DF) $\gg L$. The DF, defined as twice the Rayleigh range, is given by $2\ \pi n w_0^2/\lambda$, where $n=1.82$ stands for the YAG index of refraction and where the waist has been adjusted to $w_0 \cong 25\ \mu$m. Therefore DF $\cong 9$ mm, which is significantly larger than L. In order to put the beam waist at the crystal center, we position the focusing lens at maximum Rabi frequency, as probed by an optical nutation signal. Then we use a pinhole to select the signal emerging from the center of the illuminated spot. The sample is imaged on the 50 μm pinhole through a telescope with 4× magnification. This corresponds to an 8% peak-to-peak excitation intensity variation over the detected area. The signal is detected on an avalanche photodiode.

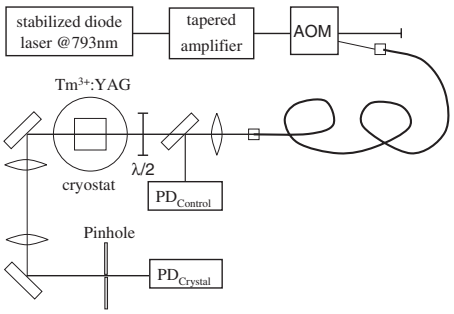

Fig. 3. Experimental setup.

The input intensity is monitored by photodetector $PD_{control}$ (Fig. 3). We carefully calibrate the detection in Rabi frequency units. This is a critical step of our experiment. Optical nutation offers the best access to Rabi frequency [14]. However this measurement technique is valid only in the low absorption limit. Because of the large sample opacity at resonance, we have to detune the laser about 20 GHz from the center of the absorption band to perform the calibration. At this spectral position the opacity is reduced by a factor of about 10. The transmitted intensity is detected on $PD_{crystal}$. We calibrate this detector with the raising edge of the rectangular pulse. Indeed, immediately after switch-on, the transmitted intensity simply reads as $I_0 \exp(-\alpha L)$, where I_0 represents the input pulse intensity that is measured on $PD_{control}$.

5. RESULTS AND DISCUSSION

We experimentally study the propagation of rectangular-shaped pulses. The pulse duration is adjusted to 7 μs, which is significantly smaller than the atomic coherence lifetime of $\cong$50 μs.

The input area ranges from 0.5 π to 3.4 π. The observed temporal profiles are displayed in Fig. 4. They exhibit the features predicted in Fig. 2. As expected, the pulse is strongly stretched around the input π area, since the area has to be conserved in spite of large resonant absorption. Then, as the input area is increased, the pulse shrinks back, which is consistent with reduced absorption. Finally, around 3 π, the pulse spreads again as reso-

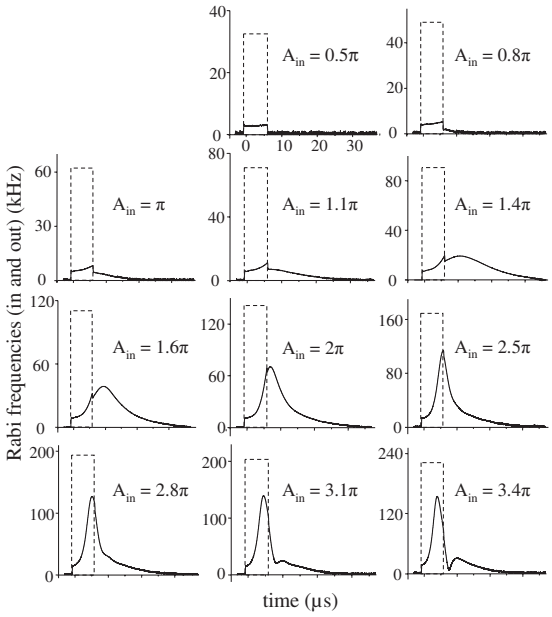

Fig. 4. Experimental profile of the transmitted pulse amplitude (solid line). Input area (A_{in}) ranges from 0.5 π to 3.4 π. Input pulses (dotted line) are rectangular with 7 μs duration.

nant absorption increases, growing a side lobe to simultaneously satisfy area conservation and energy drop.

The expected output area evolution is also observed. However, agreement with theory is only qualitative. As seen in Fig. 5 the ratio of the output area to the input area lags behind the predicted value, especially in the region of π and 3π incoming pulses. The theoretical profile in Fig. 5 accounts for the finite dipole lifetime that has been set to 50 μs. As compared with Fig. 1, the finite coherence lifetime slightly reduces the computed transmission factor, especially in the π and 3 π regions where the propagating pulse is strongly stretched. This reduction is not sufficient to fit the experiment. The value of the dipole lifetime may be questioned. With a lifetime of only 10 μs, the theoretical prediction gets closer to the experimental data. However the rising edge of the curve is shifted to higher area values, in agreement with previous works [18] but in contradiction with the experimental results.

A possible fault of the setup is the absence of antireflection coating on the crystal. As a consequence, a reflected field counterpropagates through the excited medium with an amplitude reflection coefficient as large as 30%, given the high index of refraction of YAG.

One has also to consider the failure of the plane-wave approximation when the pulse area is close to π. The plane-wave assumption relies on the large size of the depth of field with respect to the sample length and on the selection of the central part of the beam with the pinhole. However, the portions of the Gaussian beam profile corresponding to areas smaller than π are absorbed more efficiently than the central part of the beam [13]. Such a peeling of the outer portions of the beam tends to reduce the spot size and to move the waist to the output of the sample. The effective depth of field, varying as the square of the waist, gets rapidly smaller than the sample length, and since the waist migrates to the output of the sample, the imaging conditions are no longer satisfied at the pinhole position. To be more specific, let us assume that the waist moves to the end of the sample and that its size is changed from w_0 to w_0'. Let the intensity at the center of the beam profile remain unchanged. Then, provided the beam remains Gaussian, the detected intensity is reduced by the factor

$$1 + \left(\frac{L\lambda}{2\ \pi n w_0'^2} \right)^2 .$$

Changing the waist size from $w_0 = 25\ \mu$m to $w_0' = 14\ \mu$m would entail a reduction of the detected area by a factor of 2. The waist position not only moves to the output of the crystal but also undergoes strong temporal variations. This is illustrated in Fig. 6 where we simulate the time evolution of the field radial distribution. The rectangular pulse area is set equal to 1.1 π along the beam axis. We neglect the effect of diffraction. Each ray propagates at fixed distance r from the beam axis, with a well defined initial area 1.1 $\pi e^{-r^2/w^2}$. According to this model, the output spatial distribution of intensity quite faithfully replicates the input distribution, *within the incoming pulse duration*, even in the π area region. The transmitted beam distortion occurs during the delayed response of the crystal and grows dramatically as time elapses. We agree

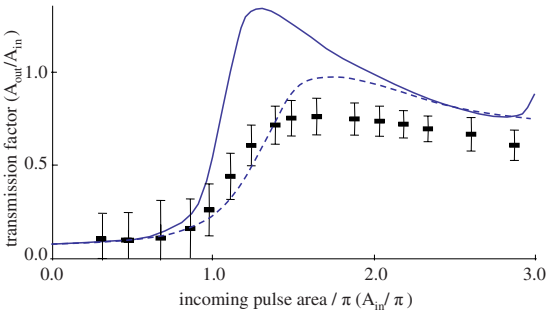

Fig. 5. (Color online) Pulse area transmission factor A_{out}/A_{in} as a function of the incoming pulse area A_{in}. Input pulses are rectangular with 7 μs duration. Theory accounts for a finite coherence lifetime of 50 μs (solid line) or 10 μs (dashed line).

this model gives nothing but a rough picture of the beam distortion. Only the 3D MB solution would correctly account for the resulting focusing and diffraction effects, but this by far exceeds the scope of the paper.

The discrepancy with theory probably results from both a coherence decay rate underestimation and violation of the large depth-of-field approximation. Finally the excess of absorption reminds us of previously reported data [15], although agreement with theory has been improved in our experiment.

6. CONCLUSION

The propagation of rectangular pulses has been investigated in monochromatic plane-wave conditions. In order to consistently account for the very broad inhomogeneous bandwidth of the absorption line, the standard MB theory has been adjusted so that the instantaneous radiative response has been described analytically. Experimental data qualitatively agree with theory. However a significant quantitative discrepancy subsists, especially in the most interesting π pulse region, where the resonantly excited Bloch vector should undergo a π rotation at any depth inside the sample [19].

In the context of quantum optical storage, the need for efficient preparation of a large optical density sample has been stressed recently [20,21]. The preparation step can

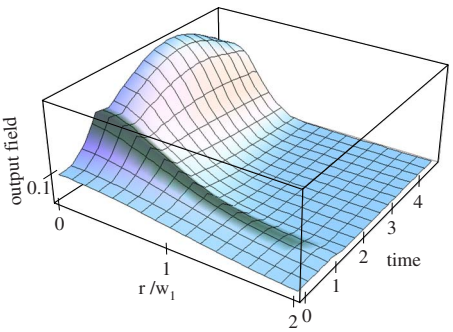

Fig. 6. (Color online) Time evolution of the radial field distribution at the crystal output. The incoming rectangular pulse with unit time duration exhibits a radial Gaussian profile with waist w_1. The field area is set equal to 1.1 π on the beam axis. The pulse reaches the crystal at time 0. Within the duration of the incoming pulse, the radial profile of the field is not strongly distorted by propagation. On the contrary, the beam radius shrinks dramatically during the delayed response of the atoms.

require sophisticated excitation procedures [22–24]. In the present paper we have concentrated on single rectangular pulse propagation as a preliminary step to the investigation of more complex pulse sequences [22]. The π pulse case deserves special attention, since all the resonantly excited ions should undergo π pulse excitation, wherever they sit in the sample depth. The unsatisfactory agreement with theory in the π pulse case should stimulate further coherent propagation investigation.

REFERENCES

1. R. H. Dicke, "Coherence in spontaneous radiation processes," Phys. Rev. **93**, 99–110 (1954).
2. N. E. Rehler and J. E. Eberly, "Superradiance," Phys. Rev. A **3**, 1735–1751 (1971).
3. S. L. McCall and E. L. Hahn, "Self-induced transparency by pulsed coherent light," Phys. Rev. Lett. **18**, 908–911 (1967).
4. R. E. Slusher and H. M. Gibbs, "Self-induced transparency in atomic rubidium," Phys. Rev. A **5**, 1634–1659 (1972).
5. R. E. Slusher, H. M. Gibbs, "Sharp-line self-induced transparency," Phys. Rev. A **6** 2326–2334 (1972).
6. S. L. McCall and E. L. Hahn, "Self-induced transparency," Phys. Rev. **183**, 457–485 (1969).
7. K.-J. Boller, A. Imamoglu, and S. E. Harris, "Observation of electromagnetically induced transparency," Phys. Rev. Lett. **66**, 2593–2596 (1991).
8. M. J. Konopnicki and J. E. Eberly, "Simultaneous propagation of short different-wavelength optical pulses," Phys. Rev. A **24**, 2567–2583 (1981).
9. S. E. Harris, "Electromagnetically induced transparency with matched pulses," Phys. Rev. Lett. **70**, 552–555 (1993).
10. V. V. Kozlov and J. E. Eberly, "Ultrashort pulses in phaseonium: the interplay between SIT and EIT," Opt. Commun. **179**, 85–96 (2000).
11. A. V. Turukhin, V. S. Sudarshanam, M. S. Shahriar, J. A. Musser, B. S. Ham, and P. R. Hemmer, "Observation of ultraslow and stored light pulses in a solid," Phys. Rev. Lett. **88**, 023602 (2001).
12. F. Schlottau, M. Piket-May, and K. Wagner, "Modelling of femtosecond pulse interaction within homogeneously broadened media using an iterative predictor corrector FDTD method," Opt. Express **12**, 182–194 (2005).
13. R. E. Slusher,"Self-induced transparency," in *Progress in Optics*, E. Wolf, ed. (North Holland, 1974), p. 55.
14. Y. Sun, G. M. Wang, R. L. Cone, R. W. Equall, and M. J. M. Leask, "Symmetry considerations regarding light propagation and light polarization for coherent interactions with ions in crystals," Phys. Rev. B **62**, 15443–15451 (2000).
15. G. Zumofen, F. R. Graf, A. Renn, and U. P. Wild, "Pulse propagation in rare-earth ion doped crystals," J. Lumin. **83–84**, 379–384 (1999).
16. C. Greiner, B. Boggs, and T. W. Mossberg, "Superradiant emission dynamics of an optically thin material sample in a short-decay-time optical cavity," Phys. Rev. Lett. **85**, 3793–3796 (2000).
17. Pierre Bouguer, Essai d'optique sur la gradation de la lumière, print. by Claude Jombert, In-12, 164 pages (1729), Paris.
18. W. Miklaszewski and J. Fiutak, "The effect of the homogeneous broadening on the propagation of the light pulses," Z. Phys. B **93**, 491–499 (1994).
19. J. Ruggiero, J.-L. Le Gouët, C. Simon, and T. Chanelière, "Why the two-pulse photon echo is not a good quantum memory protocol," Phys. Rev. A **79**, 053851 (2009).
20. Hugues de Riedmatten, Mikael Afzelius, Matthias U. Staudt, Christoph Simon, and Nicolas Gisin, "A solid-state light-matter interface at the single-photon level," Nature **456**, 773–777 (2008).
21. Mikael Afzelius, Christoph Simon, Hugues de Riedmatten, and Nicolas Gisin, "Multimode quantum memory based on atomic frequency combs" Phys. Rev. A **79**, 052329 (2009).
22. G. J. Pryde, M. J. Sellars, and N. B. Manson, "Solid state coherent transient measurements using hard optical pulses," Phys. Rev. Lett. **84**, 1152–1155 (2000).
23. F. de Seze, V. Lavielle, I. Lorgeré, and J.-L. Le Gouët, "Chirped pulse generation of a narrow absorption line in a $Tm3+:YAG$ crystal," Opt. Commun. **223**, 321–330 (2003).
24. F. de Seze, F. Dahes, V. Crozatier, F. Bretenaker, and J. -L. Le Gouët, "Coherent driving of Tm:YAG ions using a complex hyperbolic secant optical field," Eur. Phys. J. D **33**, 343–355 (2005).